Isospin-asymmetric nuclear matter

J.A. López, E. Ramírez-Homs, R. González, R. Ravelo

Department of Physics, University of Texas at El Paso, El Paso, Texas 79968, U.S.A.

(Dated: January 21, 2014)

This study uses classical molecular dynamics to simulate infinite nuclear matter and study the effect of isospin asymmetry on bulk properties such as energy per nucleon, pressure, saturation density, compressibility and symmetry energy. The simulations are performed on systems embedded in periodic boundary conditions with densities and temperatures in the ranges $\rho = 0.02$ to 0.2 fm^{-3} and T = 1, 2, 3, 4 and 5 MeV, and with isospin content of $x = Z/A = 0.3$, 0.4 and 0.5. The results indicate that symmetric and asymmetric matter are self-bound at some temperatures and exhibit phase transitions from a liquid phase to a liquid-gas mixture. The main effect of isospin asymmetry is found to be a reduction of the equilibrium densities, a softening of the compressibility and a disappearance of the liquid-gas phase transition. A procedure leading to the evaluation of the symmetry energy and its variation with the temperature was devised, implemented and compared to mean field theory results.

I. INTRODUCTION

Investigations of neutron-rich nuclei have recently attracted attention due to the advent of radioactive beam facilities [1–3]. The goal of such experimental studies is to extend what is known about the nuclear forces away from the valley of stability and in the direction of large isospin asymmetry; this is particularly important to understand the stability of radioactive nuclei and their reactions, as well as bulk properties of nuclear matter of relevance in astrophysics [4–8].

The study of the role of isospin asymmetry on nuclear forces predates current efforts. The fact that light nuclei tend to have equal numbers of protons and neutrons motivated Bethe and Weizsäcker to add an *ad hoc* term to their parametrization of the nuclear binding energy to favor the condition A=2Z, (other researchers later imposed it to the volume and surface terms [9]); such condition is attributable to the Pauli exclusion principle which lowers the overall energy of the nucleus by filling both protons and neutrons to equal levels instead of different ones. The isospin symmetric rule, however, is not satisfied in heavier nuclei ($A \gtrsim 40$) which tend to have more neutrons than protons due to a competition between the short-ranged nuclear force and the Coulomb force: in large nuclei the distance between nucleons on opposite ends of the nucleus exceeds the short-range of the attractive p-n force and thus are not be able to overcome the repulsive p-p Coulomb force unless more neutrons are added to restore stability.

This interplay between quantum and classical effects illustrates the difficulty of understanding the role of isospin symmetry in the nuclear binding energy in terms of first principles. The situation becomes more entangled in heavy-ion reactions where the nucleon energy varies with density and temperature in addition to isospin. To incorporate all of these degrees of freedom it is necessary to replace the Bethe-Weizsäcker parametrization by a full-fledged equation of state (EOS).

An intermediate compromise was based on an extension of the liquid drop formula into non-symmetric isospin values through an additive term [10], $E(\rho,\alpha) = E(\rho,\alpha=0) + E_{Sym}(\rho)\alpha^2 + O(\alpha^4)$ with $\alpha = (N-Z)/A$. Operationally such expression can be taken as a Taylor expansion of $E(\rho,\alpha)$ in terms of α about the isospin symmetric point $\alpha = 0$ with the odd-terms in α excluded due to the exchange symmetry between protons and neutrons of the strong force. Under this scheme, the symmetry term is readily obtained through $E_{Sym}(\rho) = (1/2!)(\partial^2 E/\partial\alpha^2)$ and can be analyzed as a function of the density and compared to experimental data (see e.g. [10–12]). In spite of these efforts, at present the isospin dependence of the nuclear equation of state is far from being determined; this is particularly true for the temperature dependence of E_{Sym} which has been less investigated than its zero temperature counterpart.

A more complete approach is, of course, to use microscopic theories to develop a complete equation of state with the density, temperature and isospin degrees of freedom built in from the start. Theories such as relativistic [13–19] and nonrelativistic [20, 21] Hartree Fock approximations, as well as relativistic [22] and non-relativistic mean-field models[23–29] have been used for this purpose at T=0 with varying degrees of success; the reader is directed to [30, 31] for a comprehensive review of the use of these techniques in the study of the symmetry energy term. In a nutshell, the knowledge we have about the properties of asymmetric nuclear matter is as good as the techniques used for solving the nuclear many-body problem, which are far from perfect.

A way around these technical difficulties is through the use of numerical methods like Monte Carlo, molecular dynamics, lattice calculations, etc. which are able to construct systems from which the wanted properties of nuclear matter can be obtained phenomenologically. Transport-theory models that have been used in nuclear reactions can be divided into classical, semiclassical or quantum. Synoptically, semiclassical models (BUU, IBUU, etc., see e.g. [32]) track the time evolution of the Wigner function under a mean potential to obtain a description of the probability of finding a particle at a point in phase space. On the quantum side, the molecular dynamics models (QMD, AMD, IQMD, etc., see e.g. [33–35]) solve the equations of motion of nucleon wavepackets moving within mean fields (derived from Skyrme potential energy density functional) with a Pauli-like blocking mechanism imposed and using isospin-dependent nucleon-nucleon cross sections, momentum dependence interactions, etc. Although these methods succeed in presenting a reasonable evolution of density fluctuations in heavy-ion reactions, they both fail to produce clusters of appropriate quality or quantity [32], and their use of hidden adjustable parameters (width of wavepackets, number of test particles, modifications of mean fields, effective masses and cross sections, etc.) makes their findings questionable at best. As before, practitioners of this field conclude that more detailed analysis for the equation of state is needed for the nuclear and the astrophysical community[36].

On the other hand, classical molecular dynamics (CMD) models have been used to study nuclear reactions since decades ago [37–40] and neutron star crusts more recently [41–47]. Generally speaking nucleons are treated as classical particles interacting through pair potentials with their equations of motion solved numerically with any of the several methods available, without any adjustable parameters and including all particle correlations at all levels, i.e. 2-body, 3-body, etc. Indeed the method can describe nuclear systems ranging from highly correlated cold nuclei (such as two approaching heavy ions in their ground state), to hot and dense nuclear matter (nuclei fused into an excited blob), to phase transitions (fragment and light particle production), to hydrodynamics flow (after-breakup expansion) and secondary decays (nucleon and light particle emission). The only apparent disadvantage of the CMD is the lack of quantum effects, such as the Pauli blocking, which at very low excitation energies stops the method from describing nuclear structure correctly; fortunately, in collisions the high energy deposition opens widely the phase space available for nucleons and renders Pauli blocking practically obsolete.

Thus the motivation of this study, to use CMD as a computational many-body technique to simulate infinite nuclear systems with varying density, temperature and isospin content to extricate the isospin dependence of as many nuclear characteristics as possible. In the following section the model used to obtain the energy, pressure, saturation density, compressibility and symmetry energy of infinite nuclear systems at different values of isospin, density and temperature will be presented. An overview of the resulting bulk properties of the systems studied is presented in Section III, followed by a discussion of the existence of phases in asymmetric matter in Section IV, an estimation of the nuclear symmetry energy in Section V, a discussion of the limit of applicability of the classical model in section VI and a summary of findings in Section VII.

II. CLASSICAL MOLECULAR DYNAMICS

In this work we use a CMD model with the Pandharipande potentials which were designed by the Urbana group to reproduce experimental cross sections in nucleon-nucleon collisions of up to 600 MeV [38], to mimic infinite systems with realistic binding energy, density and compressibility and to produce heavy-ion dynamics comparable to those predicted by the Vlasov-Nordheim equation. This parameter-free model has been successfully used to study nuclear reactions obtaining mass multiplicities, momenta, excitation energies, secondary decay yields, critical phenomena and isoscaling behavior that have been compared to experimental data [48–57]. More recently, and of interest to the present work, the model was used to study infinite nuclear systems at low temperatures [58] and in neutron star crust environments [45–47].

The Pandharipande potentials are comprised of an attractive potential between a neutron and a proton: $V_{np}(r) = V_r exp(-\mu_r r)/r - V_r exp(-\mu_r r_c)/r_c] - V_a exp(-\mu_a r)/r - V_a exp(-\mu_a r_c)/r_c$, and a repulsive interaction between equal nucleons (nn or pp): $V_{NN}(r) = V_0 exp(-\mu_0 r)/r - V_0 exp(-\mu_0 r_c)/r_c$. The range of these potentials is limited to a cutoff radius of $r_c = 5.4$ fm after which they are set to zero. The parameters V_r, V_a, V_0, μ_r, μ_a and μ_0 were phenomenologically adjusted by Pandharipande to yield a cold nuclear matter saturation density of $\rho_0 = 0.16$ fm^{-3}, a binding energy $E(\rho_0) = -16$ MeV/nucleon and a compressibility of about 250 MeV for their "medium" model, which is the one used here.

At a difference from a previous study of nuclear matter at low temperatures [58] where this model was used to obtain a description of the equilibrium structures (i.e. the "pasta"), in the present case we are interested on creating systems with different values of isospin content that will allow us to extract the isospin dependence of physical observables such as the energy per nucleon, pressure, equilibrium density, compressibility and the symmetry energy. With this in mind, and with an eye on future studies of transport coefficients, the molecular dynamics code used is based on the

Nosé-Hoover equations of motion which add to the newtonian mechanics the effect of a heat reservoir [59].

The addition of the heat flow variable to the classical equations of motion results in the Nosé-Hoover equations of motion which can be integrated by Størmer finite differences. In principle this approach corresponds to a canonical ensemble and does not conserve energy which is added or removed by the heat reservoir; configurations in thermal equilibrium, however, can be achieved faster than with the usual microcanonical formalism of newtonian mechanics and an Andersen's thermostat [60].

To mimic an infinite system $A = 2000$ nucleons were placed in cubic cells under periodic boundary conditions. We focus on systems with isospin content of $x = Z/A = 0.3$, 0.4 and 0.5, where Z is the number of protons. The number densities were enforced by placing the nucleons in cubical boxes with sizes selected to adjust the density. The temperatures of the systems studied are T = 1, 2, 3, 4, and 5 MeV, and their densities were selected to be around and below the corresponding saturation densities values, which vary with isospin content and temperature. The procedure followed is straightforward: the nucleons are placed at random within the cell avoiding overlaps (i.e. interparticle distances smaller than 0.1 fm) and endowed with a Maxwell-Boltzmann velocity distribution corresponding to the desired temperature. The system then is rapidly evolved until the temperature is maintained within 1%. After reaching thermal equilibrium, the system continues evolving and its information at selected time steps (nucleon positions and momenta, energy per nucleon, pressure, temperature, density, etc.) is stored for future analysis. The calculations were carried out in the High Performance Computing Center of the University of Texas at El Paso which has a beowulf class of linux clusters with 285 processors.

III. BULK PROPERTIES OF NUCLEAR MATTER

Following the procedure outlined before, the energy per nucleon (kinetic plus potential) was calculated for systems with $x = 0.3$, 0.4 and 0.5. Figure 1 shows the variation of the energy as a function of the density at temperatures T = 1, 2, 3, 4 and 5 MeV; each point represents the average of 200 thermodynamically independent configurations, the average of the standard deviations is 0.036 MeV which is smaller than the points used. In all cases the curves show the characteristic "∪" shapes around their corresponding saturation density (minimum of the ∪). It is easy to see that bound matter (i.e. with negative binding energy) exists in all three isospin cases although at high temperatures the systems become unbound. Also seen in the plots is a departure from the ∪ shapes at low densities signaling a transitions from a uniform continuous medium around saturation densities to non-homogeneous media at subsaturation densities; this effect is clearly noticeable for $x = 0.5$ and 0.4 but not for 0.3, point which will be discussed further in the following section.

The CMD calculations also yielded the pressure of the systems at each values of (T, ρ, x). Figure 2 shows the pressure versus density curves for T=1 and 5 MeV for the three isospin contents $x = 0.3$, 0.4 and 0.5. As seen in Figs. 1 and 2, the equilibrium densities correspond to the minima of the energy-density curves as well as to the zero pressure points; we estimate the values of the saturation density through a least-squares fit of a quadratic polynomial of $E(T, \rho)$ around the minimum of each curve; Figure 3 shows the variation of the saturation density with the temperature for the three values of x. As expected, the trend for symmetric matter tends to $\rho_0 = 0.16\ fm^{-3}$ as T goes to zero as expected for infinite cold nuclear matter. The case of $x = 0.3$ appears to have a very low saturation density with little temperature variation.

The compressibility at saturation density can also be obtained from the previous fit through $K(T, \rho) = 9\rho^2 \left[\partial^2 E/\partial\rho^2\right]_{\rho_0}$. Figure 4 shows the values obtained for $K(T, \rho)$ for the cases studied; as a reference the values at T = 0 obtained in a previous work [58] are also included. As it can be seen, the compressibility decreases drastically with x, and it is further reduced (by about 30%) as T increases from 1 to 5 MeV for the systems with $x = 0.4$ and 0.5, while it remains extremely soft in the neutron-rich system of $x = 0.3$.

IV. PHASES IN ASYMMETRIC MATTER

Figure 1 shows the transition from a continuous phase to an amorphous one, this phenomenon was first pointed out for cold symmetric matter in the Thomas-Fermi calculation of Williams and Koonin [61], and was recently explored at non-zero temperatures (T<1 MeV) in a CMD microcanonical study [58] using this and two other potentials. In the case of T = 1 MeV (cf. Fig. 1) it is easy to see the transition from a smooth ∪ shape to an extraneous curve at $\rho \approx 0.10\ fm^{-3}$ for $x = 0.5$, and at $\rho \approx 0.08\ fm^{-3}$ for $x = 0.4$; the behavior persists in these systems at higher temperatures but appears to be absent for the $x = 0.3$ case. As discussed in detail for the symmetric case in [58], the smooth ∪ shape corresponds to a uniform phase (crystal-like at low temperatures and liquid-like at higher

temperatures) and the lower-density separating part signals the existence of a non-homogeneous structure (such as a "pasta" at low temperatures and a liquid-gas mixture at higher temperatures).

The different behavior of the systems with $x = 0.3$ would suggest that at low temperatures the system would never enter a liquid-gas mixture region and would always stay in a liquid-like continuous medium down to very low densities. To investigate this we examined the structures formed at T = 1 MeV through the radial distribution function (RDF) and their mass distribution.

The radial distribution function, $g(r) = \rho(r)/\rho$, (cf. Figure 5) was obtained from averaging 200 systems at T=1 MeV at a liquid density ($\rho = 0.16\ fm^{-3}$, bottom panel) and at a liquid-gas mixture density ($\rho = 0.06\ fm^{-3}$, top panel). The strengths of the nearest-neighbor peaks show that at low densities nucleons tend to be more correlated than at higher densities indicating that at $\rho = 0.06\ fm^{-3}$ the main contribution at short distances is from nucleons in droplets, while at $\rho = 0.16\ fm^{-3}$ the larger nucleon mobility reduces such correlation. This is also observed in the second-neighbor peaks which appear at the same distance for all values of x at $\rho = 0.06\ fm^{-3}$ but not at $\rho = 0.16\ fm^{-3}$ indicating again a reduced mobility of nucleons in the droplets. The growth of the second-neighbors peak over the first one for $x = 0.3$ is due to the large number of nn repulsive interactions which exceed the smaller number of np attractive interactions.

It is instructive to explore the mass distributions attained by the systems in these two density regimes. In all cases the mass distribution at $\rho = 0.06\ fm^{-3}$ showed an over-abundance of intermediate mass fragments over those obtained at $\rho = 0.16\ fm^{-3}$. Figure 6 shows that for $x = 0.3$ at T = 1 MeV the system contains more intermediate-mass droplets at $\rho = 0.06\ fm^{-3}$ than at $0.16\ fm^{-3}$ where more matter remained in a continuous medium; this figure was obtained by averaging 200 systems at similar conditions and the clusters were identified through a minimum spanning tree method.

The results presented in this section thus indicate that the transition from an homogeneous medium at near-saturation densities to a non-homogeneous one at lower densities continues to exist in asymmetric nuclear matter with $x = 0.4$ and 0.3 at low temperatures ($T \lesssim 2MeV$); in other words, phases appear to be are alive and well in these cases of high isospin asymmetry. A related observation is that these systems become unbound at temperatures as low as T = 2 MeV for $x = 0.3$; observation that is in line with previous findings of the unboundness of pure neutron matter within the nuclear Thomas-Fermi model [62], and it is probably connected to the shift of the saturation density to exceedingly low values for low x.

V. NUCLEAR SYMMETRY ENERGY

The previous scheme can be used to extract the nuclear symmetry energy through $E_{Sym}(\rho) = (1/2!)\left[\partial^2 E/\partial\alpha^2\right]_{\alpha=0}$. This can be done by inserting the α dependence into an expression of the type $E(T,\rho,\alpha) = E_1(T,\alpha)\rho + E_2(T,\alpha)\rho^2 + E_3(T,\alpha)\rho^3$ and adjusting the parameters $E_1(T,\alpha)$, $E_2(T,\alpha)$ and $E_3(T,\alpha)$ to fit the values of $E(T,\rho,x)$ for each T and x in the $\cup$ region, namely from $\rho = 0.09$ to $0.2\ fm^{-3}$ for $x = 0.4$ and 0.5, and $\rho = 0.04$ to $0.2\ fm^{-3}$ for $x = 0.3$. The resulting fits are shown as solid lines in Figure 1.

More explicitly, using the data for $x = 0.5$, 0.4 and 0.3 and remembering that $\alpha = (N - Z)/A = 1 - 2x$, it is possible to obtain, for instance, values for $E_1(T, \alpha = 0)$, $E_1(T, \alpha = 0.2)$ and $E_1(T, \alpha = 0.4)$ and approximate $E_1(T,\alpha) = E_{10}(T) + E_{12}(T)\alpha^2 + E_{14}(T)\alpha^4$, where the coefficients $E_{10}(T)$, $E_{12}(T)$ and $E_{14}(T)$ can be obtained by solving the resulting system of coupled equations. Using similar expressions for $E_2(T,\alpha)$ and $E_3(T,\alpha)$ it is simple to obtain $E_{Sym}(T,\rho) = E_{12}(T) + E_{22}(T)\rho + E_{32}(T)\rho^2$. The resulting E_{Sym} are presented in Figure 7 as a function of the density for T=1, 2, 3, 4 and 5 MeV.

The smooth dependence of E_{Sym} with the density is reminiscent of previous results obtained with microscopic field theories. For comparison we show the symmetry energy obtained by Chen at al. [31] using a relativistic Hartree calculation (curve labeled "NL_2") along with values obtained with other field theories all plotted at their corresponding saturation densities (see [31] for complete details).

Another result worth mentioning is the smooth temperature dependence of $E_{sym}(T,\rho)$ which, interestingly, has a trend opposite to previous findings. In the past the temperature dependence of E_{sym} has been studied using an equation of state obtained through a virial expansion at T = 2, 4 and 8 MeV [63], and through a self-consistent model using various effective interactions at temperatures ranging up to 50 MeV [64]; in both of these calculations an inverse temperature dependence was found, that is E_{sym} decreased as T increased. From a different perspective, the CMD results appear to be in line with those obtained by de Lima and Randrup [65] with a modified Seyler-Blanchard model, which show an overall increase of the free energy through changes of the volume and surface coefficients and nuclear surface tension in the range of $T \lesssim 5$ MeV.

It stands to reason that the differences between the CMD results and those of field theories reflect the distinct underlying assumptions of the models. A major difference is that the field theories were adapted to reproduce the

binding energies and charged radii of stable (i.e. nearly isosymmetric) finite nuclei in their ground-state while the CMD results stem out of a generalized analysis of heated infinite systems at varying isospin content. Another significant difference is that the E_{sym} extracted from the CMD results is not based on the extraneous partition of the liquid drop formula into an isospin symmetric part and an isospin asymmetric additive term; indeed the CMD results stem from the holistic effects the density, temperature and isospin dependence have on the energy simultaneously. Other differences are the amount of interactions that each method incorporates, while field theories are usually limited to the ladder diagrams, the CMD contains all many-body interactions. Fortunately, as it will be discussed in more detail in the section VI, the lack of quantum effects of CMD appears not to play a major role in the validity of these results.

However, independent of all of these differences between the models, there is another important factor. Unfortunately –or perhaps, fortunately–, the procedure used to obtain E_{sym} from the CMD results involves fitting algorithms that contain an intrinsic variability (due to the specific points included in the fit, error bars, etc.) that yields a margin to play with the fit of $E(T,\rho,\alpha)$ which in turn produces various functional forms of $E_{sym}(T,\rho)$. In fact, it is possible to work "backwards" (using multivariate regression analysis) and find relatively close fits of $E(T,\rho,\alpha)$ that produce an specific form of $E_{sym}(T,\rho)$. Figure 8, for instance, shows fits of $E(T,\rho,\alpha)$ for T = 1 MeV that fall within 0.7 MeV of the CMD data points (indicated by the data bars) and yield exactly the NL_2 symmetry energy of Figure 7. Viewing this on the positive side, these results signal a possible compatibility between the CMD results and other theories. But viewing it on the negative side, this variability effectively rules out the procedure used for an exact extraction of the nuclear symmetry energy and limits its scope to more general "ball park" estimates.

VI. QUANTUM CAVEATS

As explained in the Introduction, classical molecular dynamics lacks all quantum effects, such as the Pauli blocking, which at low excitation energies could produce an incorrect energy distribution. The question then arises, how does this deficiency of CMD affect the results of this investigation? In the Introduction it was stated that for high excitation energies the phase space available for nuclei would be so ample that it would render Pauli blocking practically obsolete. In this section such statement is quantified in a bit more detail.

Quantum effects affect the behavior of many body systems on, at least, two fronts: energy distribution and wave mechanics. From the point of view of the energy, in bound clusters the energy of individual nucleons becomes discrete and the distribution of energy levels is ruled by Fermi-Dirac statistics with Pauli exclusion principle further regulating the occupation of such levels. As stated before, at high excitation energies the density of states becomes so finely dense that Pauli blocking is rendered obsolete, such limit can be said to exist whenever the number of quantum states available to a nucleon at a given temperature is much greater than the number of nucleons. According to statistical mechanics this previous condition is $\Phi(\epsilon) \gg N$ and, for the simple case of a particle in a box where $\Phi(\epsilon) = \frac{\pi V}{6}\left(\frac{8M\epsilon}{h^2}\right)^{3/2}$ and $\epsilon = 3T/2$, it can be approximated by [66]

$$N/\Phi(\epsilon) = \sqrt{\frac{\pi}{6}}\frac{\rho h^3}{(2\pi MT)^{3/2}} \ll 1 \ , \tag{1}$$

where M is the nucleon mass and ρ is the neutron or proton number densities at saturation. Using the values of ρ from Figure 3 along with $\rho_n = (1-x)\rho$ and $\rho_p = x\rho$ for neutrons and protons respectively, $N/\Phi(\epsilon)$ yields the values shown in Figure 9, which demonstrate that condition (1) is fully satisfied in all of the cases considered in this study except, perhaps, for $x \geq 0.4$ at T $\approx$ 1 MeV where $N \gtrsim \Phi(\epsilon)$ and the condition is marginally satisfied.

A second test of the validity of the classical approach has to do with the wave features of the particles. It is known that wave mechanics yields to classical mechanics whenever the mean inter-particle distance is much larger than the mean thermal de Broglie wavelength λ_T. Using $(V/N)^{1/3} = \rho^{-1/3}$ as the inter particle distance, this condition yields to the inequality [67]

$$\rho\lambda_T^3 = \frac{\rho h^3}{(2\pi MT)^{3/2}} \ll 1 \ . \tag{2}$$

We notice that condition (2) is practically identical to condition (1) except for a small numerical factor of order 1. In this case, however, M stands for the nuclei masses and ρ for the overall system's density. Figure 10 shows the values of $\rho\lambda_T^3$ as a function of density and for masses A = 1 (top band) and 10 (lower band). The shaded regions indicate the values obtained for each of the two masses for the range of temperatures 1 MeV $\leq$ T $\leq$ 5 MeV; higher masses produce bands with values of $\rho\lambda_T^3$ that are even smaller. It is easy to see that condition (2) is fully satisfied by all size particles at all of the densities and temperatures considered in the present study except, perhaps, for free nucleons at T $\approx$ 1 MeV and $\rho > 0.1\ fm^{-3}$ where $\rho\lambda_T^3 \approx 1$ and the condition is marginally satisfied.

Figures 9 and 10 thus provide a degree of confidence over the CMD results. Indeed Fig. 9 provides certainty over the energy distribution attained by nucleons in nuclei near saturation density, while Fig. 10 confirms the validity of the dynamics of the system (and hence its thermodynamics) in the liquid-gas phase. Other quantum effects, such as collective excitations, superfluidity and superconductivity, etc. are known to occur at lower temperatures, near the ground state of the nucleus, and are unlikely to affect the results of the present calculation.

VII. CONCLUDING REMARKS

In this study we used CMD to simulate infinite nuclear systems with varying density, temperature and isospin content to extract the isospin dependence of the energy per nucleon, pressure, saturation density, compressibility and symmetry energy. We studied systems with 2000 nucleons embedded in periodic boundary conditions with densities and temperatures in the ranges $\rho = 0.02$ to 0.2 fm^{-3} and T = 1, 2, 3, 4 and 5 MeV, and with isospin content of $x = Z/A = 0.3$, 0.4 and 0.5.

The results obtained for the energy per nucleon (cf. Fig. 1) indicate that symmetric ($x = 0.5$) and asymmetric matter ($x = 0.3$ and 0.4) can be self bound for certain values of T and ρ. The equilibrium densities obtained from the minima of the energy-density curves indicate that as T increased from 1 to 5 MeV, the saturation densities varied from $\rho_0 = 0.16$ fm^{-3} to 0.12 fm^{-3} for isospin symmetric matter, and from $\rho_0 \approx 0.12$ fm^{-3} to 0.09 fm^{-3} for matter with $x = 0.4$.

The compressibility around saturation density was determined from the $E(T, \rho)$ data and it was found that isospin asymmetry softens nuclear matter by a factor of about 50% as x drops from 0.5 to 0.4 or from 0.4 to 0.3. It was also observed that the compressibility is further reduced (by about 30%) as T increases from 1 to 5 MeV for the systems with $x = 0.4$ and 0.5.

The existence of phases was identified by examining the density dependence of the energy per nucleon. At all isospin asymmetries the energy $E(T, \rho)$ showed $\cup$ shapes around the saturation densities characteristic of a continuous liquid-like phase. At sub-saturation densities the energy-density curves of $x = 0.4$ and 0.5 departed from the uniform liquid phase signaling a transition to a non-homogeneous one, presumably a liquid-gas mixture.

The larger asymmetric case of $x = 0.3$ deserves a special mention. Such systems become unbound at all densities for temperatures as low as T = 3 MeV, and exhibited very low saturation densities and extremely small compressibility at all temperatures. These assertions were ratified by the measurements of the the zero-pressure densities (cf. Figure 2). Although these findings would suggest that at low temperatures the system would never enter a liquid-gas mixture region and would always stay in a liquid-like continuous medium down to very low densities, a close examination of the structures formed at T = 1 MeV through the radial function and mass distribution at $\rho = 0.06$ and $\rho = 0.16$ fm^{-3} indicate that phases are alive and well in this highly isospin symmetric case.

Turning now to the nuclear symmetry energy, a procedure to obtain $E_{Sym}(T, \rho)$ from the CMD values of $E(T, \rho, \alpha)$ was devised and implemented. The results show both a smooth dependence of the symmetry energy with the density and the temperature. Unfortunately, the statistical variations of the energy density are not small enough as to pinpoint the symmetry energy with satisfactory accuracy.

Comparing to previous studies, our dynamical results confirm certain previous predictions while extending them to higher temperatures or other values of isospin asymmetry. For instance, the shapes of $E(T, \rho, \alpha)$ resemble closely the predictions of Skyrme-Hartree-Fock and relativistic mean-field calculations for zero temperature [68]. Likewise, the softening of K with excitation energy appears to be consistent with IQMD calculations of intermediate-mass fragments multiplicities in simulations of $^{197}Au + ^{197}Au$ at 600 MeV/A [36] and with BUU calculations of the traverse component of the elliptic flow of similar reactions at 1 GeV/A [6], both observables presumably correspond to higher excitations. As mentioned before, the low binding energy of $x = 0.3$ matter is in line with the lack of binding of neutron-rich [68] and pure neutron matter [62] at zero temperature.

Along the same lines, our results for the symmetry energy are reminiscent of relativistic and non-relativistic Hartree calculations [31] and, in fact, can be made to fully agree with such calculations. Characteristics such as the temperature dependence of $E_{sym}(T, \rho)$ appear to be in agreement with the variations of liquid-drop terms and nuclear surface tension in the range of $T \lesssim 5$ MeV [65] but in disagreement with trends obtained by other theories [63, 64].

In summary, the CMD model indeed helps to understand the role of isospin on several nuclear properties. Besides corroborating previous studies, this work extends some of their results to other values of isospin content and non-zero temperatures. Findings that we believe are new are the temperature variation of the saturation density and compressibility for isospin asymmetric matter, certain details of the existing phases at $x = 0.3$ and 0.4, as well as a new procedure to estimate $E_{sym}(T, \rho)$ from kinetic simulations.

In the future this study will be extended to lower temperatures (where crystalline structures exist) and other transport properties such as speed of sound, diffusion coefficients, and to finite systems.

ACKNOWLEDGMENTS

This study was financed by the National Science Foundation grant NSF-PHY 1066031 and by DOE's Visiting Faculty Program. The authors acknowledge helpful conversations with Jørgen Randrup and thank the warm hospitality of the Nuclear Theory Group of the Nuclear Science Division of The Lawrence Berkeley National Laboratory where this work was carried out from beginning to end.

REFERENCES

[1] HIRFL, see W. Zhan et al., Int. Jour. Mod. Phys. E 15, 1941 (2006).
[2] RIKEN, see Y. Yano, Nucl. Instr. Meth. B261, 1009 (2007).
[3] GSI-Fair, see https://www.gsi.de/en/research/fair.htm.
[4] B.A. Li, C.M. Ko and W. Bauer, topical review, Int. Jour. Mod. Phys. E 7, 147 (1998).
[5] Isospin Physics in Heavy-Ion Collisions at Intermediate Energies, Eds. Bao-An Li and W. Udo Schroder (Nova Science Publishers, Inc, New York, 2001).
[6] P. Danielewicz, R. Lacey and W.G. Lynch, Science 298, 1592 (2002).
[7] J.M. Lattimer and M. Prakash, Phys. Rep. 333, 121 (2000); *ibid*, Astrophys. J. 550, 426 (2001); *ibid*, J.M. Lattimer and M. Prakash, Science 304, 536 (2004).
[8] A.W. Steiner, M. Prakash, J.M. Lattimer and P.J. Ellis, Phys. Rep. 411, 325 (2005)
[9] W.D. Myers and W.J. Swiatecki, Nucl. Phys. **A81**, 1 (1966).
[10] M.B. Tsang, et al., Phys Rev Lett. 102, 122701 (2009).
[11] W. Trautmann et al, Int. J. Mod. Phys. **E19**, 1653 (2010).
[12] J.B. Natowitz, G. R opke, S. Typel, D. Blaschke, A. Bonasera, K. Hagel, T. Kl ahn, S. Kowalski, L. Qin, S. Shlomo, R. Wada and H.H. Wolter, PRL **104**, 202501 (2010).
[13] S. Ulrych and H. Muther, Phys. Rev. **C56**, 1788 (1997).
[14] E.N.E. van Dalen, C. Fuchs and A. Faessler, Nucl. Phys. **A741**, 227 (2004).
[15] Z.Y. Ma, J. Rong, B.Q. Chen, Z.Y. Zhu and H.Q. Song, Phys. Lett. **B604**, 170 (2004).
[16] F. Sammarruca, W. Barredo and P. Krastev, Phys. Rev. **C71**, 064306 (2005).
[17] E.N.E. van Dalen, C. Fuchs, and A. Faessler, Phys. Rev. Lett. **95**, 022302 (2005).
[18] E.N.E. van Dalen, C. Fuchs, and A. Faessler, Phys. Rev. **C72**, 065803 (2005).
[19] J. Rong, Z.Y. Ma, and N. Van Giai, Phys. Rev. **C73**, 014614 (2006).
[20] I. Bombaci and U. Lombardo, Phys. Rev. **C44**, 1892 (1991).
[21] W. Zuo, L.G. Cao, B.A. Li, U. Lombardo, and C.W. Shen, Phys. Rev. **C72**, 014005 (2005).
[22] V. Baran, M. Colonna, V. Greco, and M. Di Toro, Phys. Rep. **410**, 335 (2005).
[23] C.B. Das, S. Das Gupta, C. Gale, and B.A. Li, Phys. Rev. **C67**, 034611 (2003).
[24] B.A. Li, C. B. Das, S. Das Gupta, and C. Gale, Phys. Rev. **C69**, 011603(R) (2004); Nucl. Phys. **A735**, 563 (2004).
[25] B.A. Li, Phys. Rev. **C69**, 064602 (2004).
[26] L.W. Chen, C.M. Ko, and B.A. Li, Phys. Rev. **C69**, 054606 (2004).
[27] J. Rizzo, M. Colonna, M. Di Toro, and V. Greco, Nucl. Phys. **A732**, 202 (2004).
[28] B. Behera, T.R. Routray, A. Pradhan, S.K. Patra, and P.K. Sahu, Nucl. Phys. **A753**, 367 (2005).
[29] J. Rizzo, M. Colonna, and M. Di Toro, Phys. Rev. **C72**, 064609 (2005).
[30] B.A. Li, L.W. Chen and C.M. Ko, Phys. Rep. **464**, 113 (2008).
[31] L.W. Chen, C.M. Ko and B.A. Li, Phys. Rev. **C76**, 054316 (2007).
[32] M.A. Famiano1, T. Liu, W. G. Lynch, M. Mocko, A. M. Rogers, M. B. Tsang, M.S. Wallace, R. J. Charity, S. Komarov, D. G. Sarantites, L.G. Sobotka and G. Verde, Phys. Rev. Lett. **97**, 052701 (2006).
[33] A. Ono, H. Horiuchi, H. Takemoto and R. Wada, Nuc. Phys. **A630**, 148 (1998).
[34] K. Singh Vinayak and S. Kumar, J. Phys. G: Nucl. Part. Phys. **39** 095105 (2012).
[35] S. Kumar and Y.G. Ma, Phys. Rev. **C86**, 051601R (2012).
[36] S. Kumar and Y.G. Ma, Nuc. Phys. **A898**, 57 (2013).
[37] L. Wilets, E.M. Henley, M. Kraft and A.D. Mackellar, Nuc. Phys. **A282**, 342 (1977)
[38] A. Vicentini, G. Jacucci and V.R. Pandharipande, Phys. Rev. **C31**, 1783 (1985); R. J. Lenk and V. R. Pandharipande, Phys. Rev. **C34**, 177 (1986); R.J. Lenk, T.J. Schlagel and V. R. Pandharipande, Phys. Rev. **C42**,372 (1990).
[39] J.A. López and G. Lübeck, Phys. Lett. **B219**, 215 (1989).
[40] C.O. Dorso and J. Randrup, Phys. Lett. **B301**, 328 (1993).

[41] C.J. Horowitz, M.A. Pérez-García, and J. Piekarewicz, Phys. Rev. **C69**, 045804 (2004).
[42] C.J. Horowitz, M.A. Pérez-García, J. Carriere, D.K. Berry, and J. Piekarewicz, Phys. Rev. **C70**, 065806 (2004).
[43] C.J. Horowitz, M.A. Pérez-García, D.K. Berry, and J. Piekarewicz, Phys. Rev. **C72**, 035801 (2005).
[44] J. Piekarewicz and G. Toledo Sánchez, Phys. Rev. **C85**, 015807 (2012).
[45] C.O. Dorso, P.A. Giménez Molinelli and J.A. López, in "Neutron Star Crust", Eds. C.A. Bertulani and J. Piekarewicz, Nova Science Publishers, ISBN 978-1620819029 (2012).
[46] C.O. Dorso, P.A. Giménez Molinelli and J.A. López, Phys. Rev. **C86**, 055805 (2012).
[47] J.A. López, E. Ramírez-Homs, C.O. Dorso and P.A. Giménez Molinelli, to be published (2012).
[48] A. Barrañón, C.O. Dorso, J.A. López and J. Morales, Rev. Mex. Fís. **45**, 110 (1999).
[49] A. Chernomoretz, L. Gingras, Y. Larochelle, L. Beaulieu, R. Roy, C. St-Pierre and C. O. Dorso, Phys. Rev. **C65**, 054613 (2002).
[50] A. Barrañón, C.O. Dorso and J.A. López, Rev. Mex. Fís. **47-Sup. 2**, 93 (2001).
[51] A. Barrañón, C.O. Dorso, and J.A. López, Nuclear Phys. **A791**, 222 (2007).
[52] A. Barrañón, R. Cárdenas, C.O. Dorso, and J.A. López, Heavy Ion Phys. **17**, 1, 41 (2003).
[53] C.O. Dorso and J.A. López, Phys. Rev. **C64**, 027602 (2001).
[54] A. Barrañón, J. Escamilla Roa and J.A. López, Braz. J. Phy., **34-3A** 904 (2004).
[55] A. Barrañón, J. Escamilla Roa and J.A. López, Phys. Rev. **C69**, 014601 (2004).
[56] C.O. Dorso, C.R. Escudero, M. Ison and J.A. López, Phys. Rev. **C73**, 044601 (2006).
[57] C.O. Dorso, P.A. Giménez Molinelli and J.A. López, J. Phys. G: Nucl. Part. Phys. **38** 115101 (2011); *ibid*, Rev. Mex. Phys., **S 57 (1)**, 14 (2011).
[58] C.O. Dorso, P.A. Giménez Molinelli, J.I. Nichols and J.A. López, submitted to Nuc. Phys. (2013).
[59] B.L. Holian, A.F. Voter and R. Ravelo, Phys. Rev. **E52**, 2338 (1995).
[60] H.C. Andersen, J. Chem. Phys. **72** 2384 (1980).
[61] R.D. Williams and S.E. Koonin, Nuc. Phys. **A435**, 844 (1985).
[62] W.D. Myers and W.J. Swiatecki, Acta Phys. Pol. **B**26, 111 (1995)
[63] C.J. Horowitz, A. Schwenk, Nucl. Phys. **A**776, 55-79 (2006).
[64] J. Xu, L.W. Chen, B.A. Li, H.R. Ma, Phys. Rev. **C**75, 014607 (2007).
[65] E. de Lima Medeiros and J. Randrup, Phys. Rev **C45** 372 (1992).
[66] D.A. McQuarrie, Statistical Thermodynamics, University Science Books, (2000).
[67] C. Kittel and H. Kroemer, Thermal Physics (2 ed.), W. H. Freeman. p. 73, (1980).
[68] I. Tanihata, Preprint RIKEN-AF-NP-229, 1996.

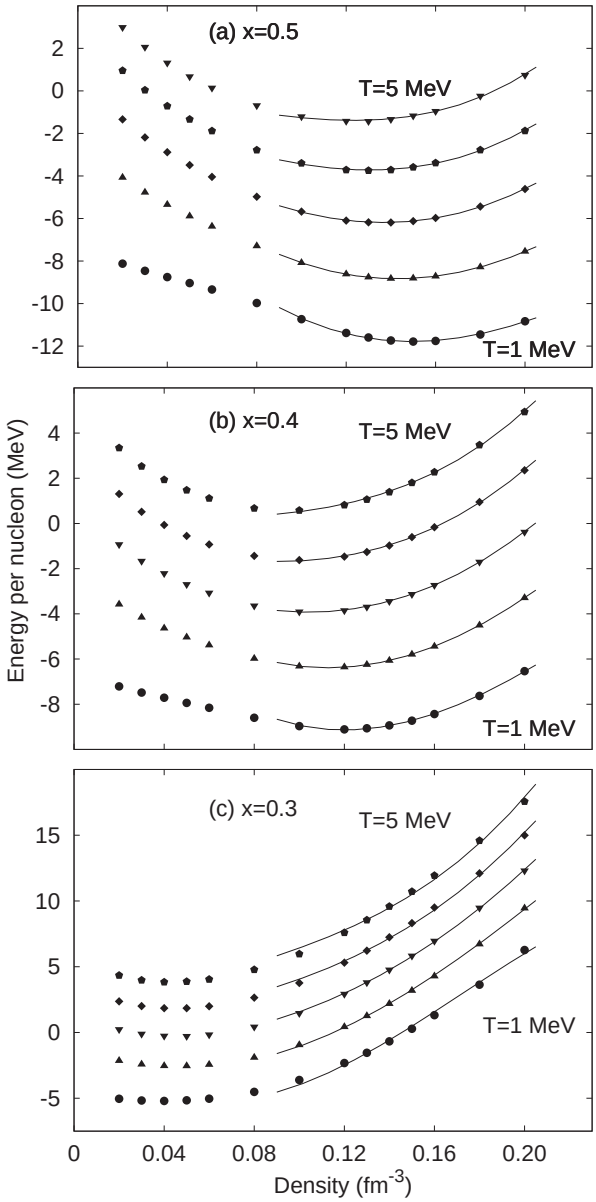

FIG. 1: Energy per nucleon as a function of the density for three different isospin contents. In each case the curves correspond to temperatures ranging from T = 1 MeV (lower curve) to 5 MeV (upper curve) with the intermediate curves corresponding to 2, 3 and 4 MeV. The lines indicate the fits used in Section V to estimate the symmetry energy.

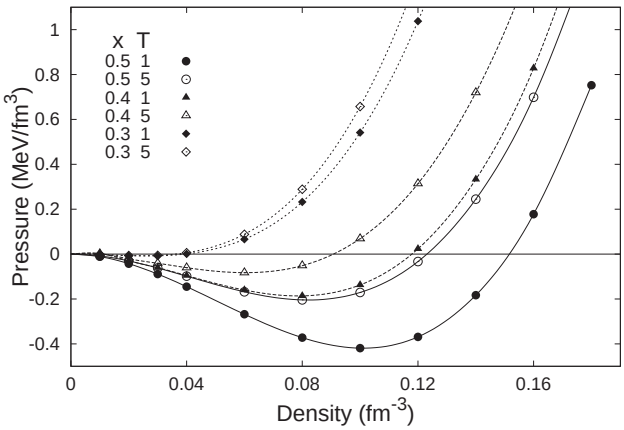

FIG. 2: Values of the pressure obtained in the molecular dynamics simulations presented as a function of the density for three different isospin contents and T = 1 and 5 MeV.

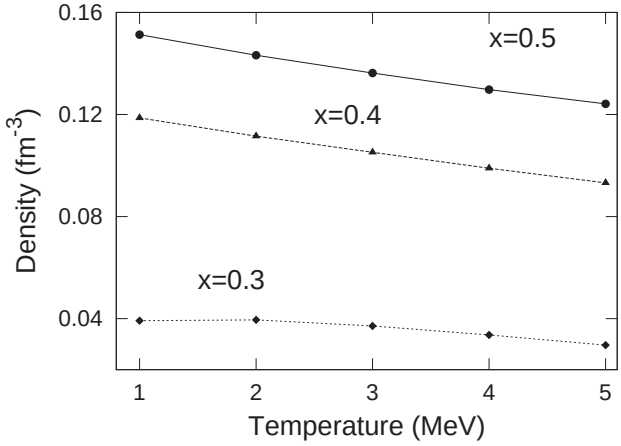

FIG. 3: Saturation density as a function of the temperature for three different isospin content.

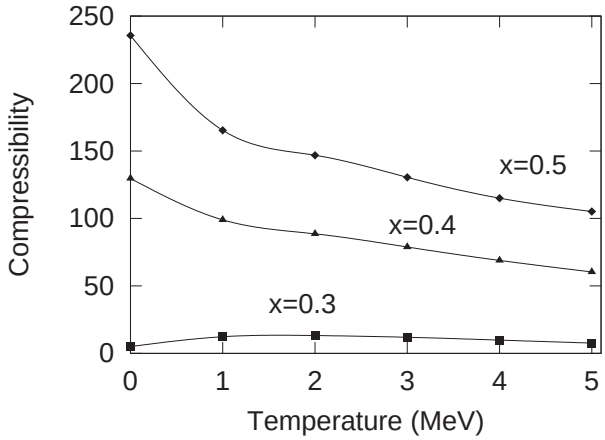

FIG. 4: Compressibility as a function of the temperature for three different isospin content.

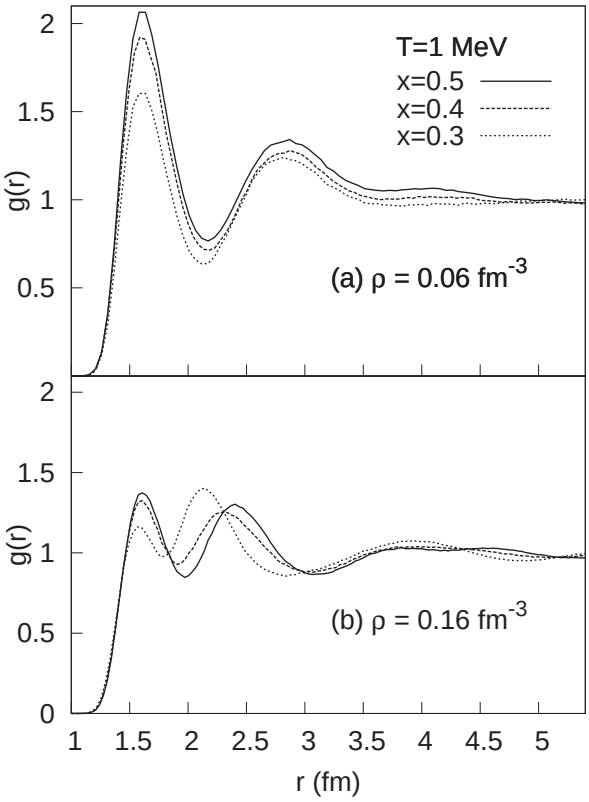

FIG. 5: Radial distribution functions of systems with $x = 0.3$, 0.4 and 0.5 at T = 1 MeV and densities $\rho = 0.06\ fm^{-3}$ in panel (a) and $\rho = 0.16\ fm^{-3}$ in panel (b).

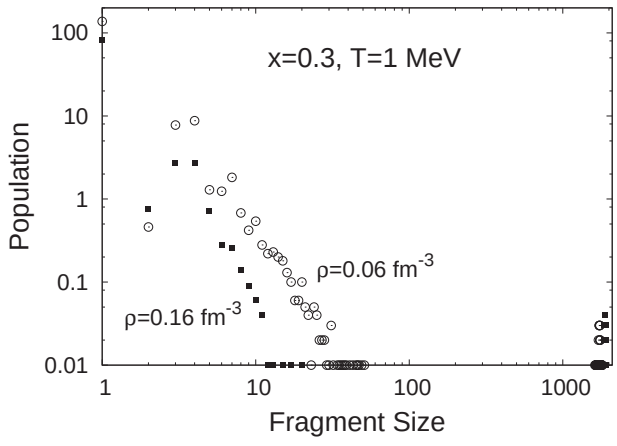

FIG. 6: Mass distribution obtained with $x = 0.3$, T = 1 MeV at $\rho = 0.06$ and $0.16\ fm^{-3}$.

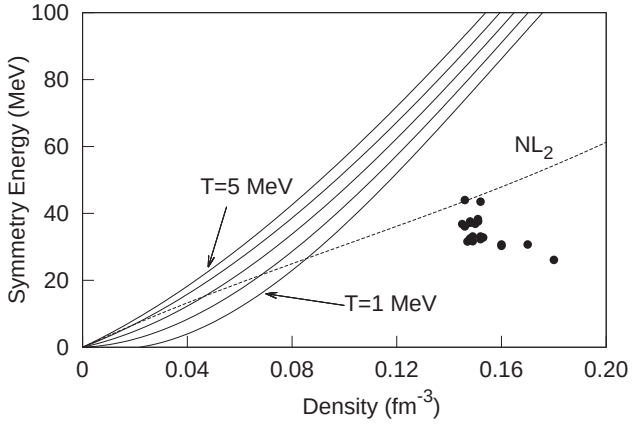

FIG. 7: The solid lines show the symmetry energies obtained from the CMD values of $E(T, \rho, \alpha)$ for T = 1, 2, 3, 4 and 5 MeV as explained in the text. For comparison, the dashed line (NL_2) and the points all show values of the symmetry energy obtained with different relativistic Hartree calculations.

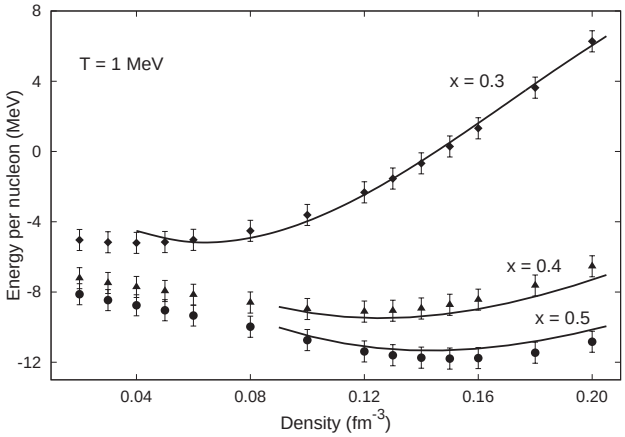

FIG. 8: The lines show the fits of $E(T, \rho, \alpha)$ for T=1 MeV that lead to a symmetry energy identical to NL_2 in Fig, 7.

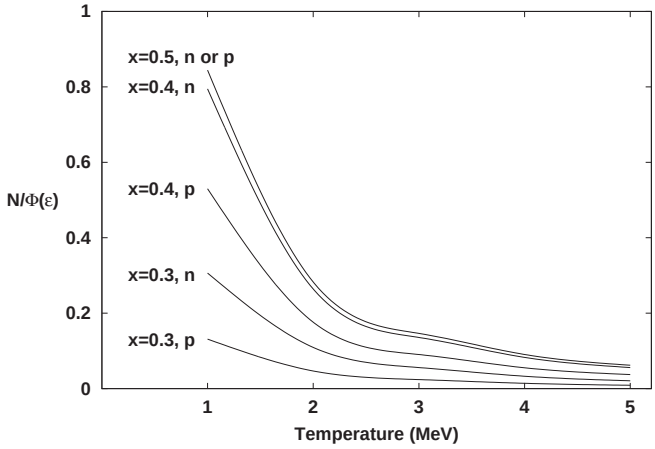

FIG. 9: Values of $N/\Phi(\epsilon)$ as a function of temperature for $x = 0.3$, 0.4 and 0.5 and for protons (p) and neutrons (n).

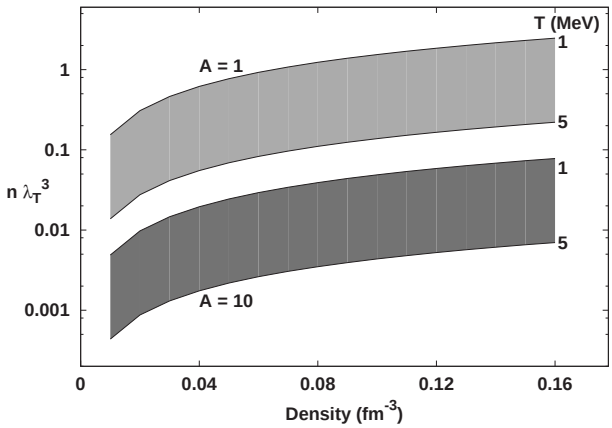

FIG. 10: Values of $\rho\lambda_T^3$ as a function of density and for a range of temperatures and for two values of the masses.